Pergamon

*Radiat. Phys. Chem.* Vol. 51, No. 4–6, pp. 689–700, 1998

Printed in Great Britain

PII: S0969-806X(97)00241-7

0969-806X/98 $19.00 + 0.00

# NON-DESTRUCTIVE ANALYSIS OF ANCIENT METAL ALLOYS BY IN SITU EDXRF TRANSPORTABLE EQUIPMENT

G. E. GIGANTE[1] and R. CESAREO[2]

[1]Dipartimento di Fisica, Università di Roma, La Sapienza, Piazza A. Moro, 8, Rome, Italy and
[2]Istituto di Matematica e Fisica, Università di Sassari, Sassari, Italy

**Abstract**—The availability of transportable equipment for in situ non-destructive analysis of works of art is considered to be very important. In situ non-destructive study is typically diagnostic, therefore requiring only qualitative or semiquantitative results. In the case of alloys, quantitative results can also be obtained. In Energy Dispersive X-Ray Fluorescence (EDXRF) analysis, portable instruments can now be assembled. For instance, miniaturised X-ray tubes with air cooling and high resolution semiconductor detectors thermoelectrically cooled are now available, allowing the construction of completely transportable apparatus for EDXRF analysis. In this work, aspects regarding methodology of analysis and discussion of the precision obtainable in analysis of ancient metals are presented. © 1998 Elsevier Science Ltd. All rights reserved

## INTRODUCTION

Archaeometry and conservation can be viewed as experimental branches of historical disciplines. In these fields, Energy Dispersive X-Ray Fluorescence (EDXRF) has found extensive use because it is a non-invasive technique which makes possible the detection of the elemental profile of inorganic materials, such as those constituting objects of art. Among the most significant applications of EDXRF in these fields are the quantitative analysis of alloys and the non-destructive study of inorganic pigments in paintings and frescoes.

EDXRF is a well known technique in applied fields since it offers a number of notable advantages, including simplicity. Since the 1980s, transportable/portable equipment have been developed using radioisotopic sources and proportional gas counters and scintillators (Cameron and Rhodes, 1961; Cesareo *et al.*, 1972). Unfortunately, use of these was limited by the poor energy resolution of the detectors and problems associated with the transportation of radioisotopic sources. The possibility of assembling transportable systems with adequate characteristics has only recently been realised due to (i) the development of cryoelectrically cooled detectors with improved energy resolution (Cesareo *et al.*, 1992; Wang *et al.*, 1993; Huber *et al.*, 1994) and (ii) the realisation of dedicated X-ray tubes of small dimensions and adequate stability (Cesareo *et al.*, 1996a,b; Oxford, 1996).

There is substantial difference between a transportable and a real portable spectrometer: a portable instrument must be autonomous, i.e. complete with its own battery, and its weight must be sufficiently small that it can be positioned by hand without the aid of other support, while a transportable instrument can be brought to the chosen site for measurements.

For most applications it is enough to have a transportable rather than a portable system. Indeed, in the case of works of art the problem is really one of not being allowed to take samples, and therefore a spectrometer is required which can be moved in order to analyse desired points on the object.

There exist a large number of systems for non-destructive analysis of materials, but only a few have been constructed such that the equipment can be transported to museums or excavation sites, with the advantage of both not needlessly damaging the work of art and of not moving it. To move a work of art is, in fact, very complex for both bureaucratic and security reasons. In particular, the security reasons take into account the two risks that the work of art (i) could be stolen and (ii) could suffer damage. In addition, to transfer a work of art is an extremely costly operation. Thus, the use of equipment which can be moved can drastically reduce the cost of investigation and favour greater use of such scientific methods in the study (including assay before and during restoration) of a work of art.

The basic components of the EDXRF apparatus (see Fig. 1) are: (a) an X-ray source; (b) an X-ray detector; (c) an electronic system including data acquisition, storage and data presentation. The transportable EDXRF equipment used in the field of archaeometry and conservation are of two types:

1. for large works of art, such as paintings, frescos, large metal artefacts, large ceramic items, etc. an

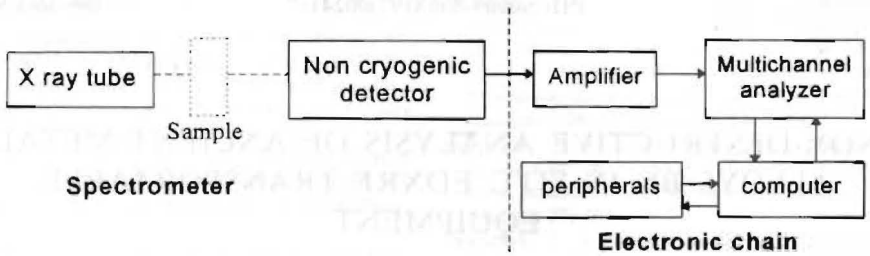


Fig. 1. Diagram of a typical portable spectrometer.

EDXRF spectrometer fixed on a moveable platform for the positioning of the measuring system in front of the work of art;

2. for small works of art, such as small metal artefacts, small painted surfaces (miniatures, water-colour, jewels), etc. a fixed spectrometer equipped with a moveable support for the positioning of the work of art in front of the spectrometer.

Metals are especially suited to EDXRF analysis. The high atomic number ($Z$) and density of metals can facilitate the obtaining of high intensity secondary X-ray lines, even when making use of low intensity sources. Moreover, in the case of metal alloys emission lines of all the elements included in the alloy can be detected.

The strong self-absorption of the radiation emitted by the sample is an inherent limiting factor because this produces non-linearity in the response of the measuring system. Given the assumption of homogeneous samples, there exists the possibility of correcting the non-linear response by using the fundamental parameter method.

The non-homogeneity of samples is an additional limiting factor; in particular ancient metal artefacts are characterised by a superficial layer which is due to (i) the effect of external agents (patina) or (ii) to superficial treatment. In addition, the bulk material is characterised by a microstructure, this sometimes being due to the fusion technique; these grains or lamellae, if enriched with higher-$Z$ elements, can strongly absorb the fluorescence radiation.

In this work, the theoretical framework for non-destructive study of ancient metal artefacts is discussed, as are the measurements carried out using transportable equipment, during recent archaeometric campaigns in Italian archaeological museums.

## APPROACHES TO THE QUANTITATIVE X-RAY FLUORESCENCE ANALYSIS OF ANCIENT METAL ARTEFACTS

### *Basic equations for quantitative X-ray fluorescence analysis*

The fluorescence intensity $N_a$ (net number of counts detected in a given spectral window) produced by the atoms of an element **a** within a uniform sample irradiated with a monochromatic beam of energy $E_0$ and intensity $N_0^i$ is given by:

$$N_a = N_0 k \epsilon(E_a) \mu_{ph,a}(E_0) \omega_{a,s} F_{a,s} p_l w_a \times \frac{1 - e^{-\left[\mu(E_0)+\mu(E_a)\right]\rho x}}{\mu(E_0) + \mu(E_a)} \quad (1)$$

where:

$k$ is a geometrical term, depending on the source–sample and sample–detector distances and on the detector area;

$\epsilon(E_a)$ is the intrinsic detector efficiency for the particular energy of the fluorescence line of the element **a**;

$\mu_{ph,a}(E_0)$ represents the photoelectric mass attenuation coefficient of element **a** at incident energy $E_0$;

$\omega_{a,s}$ is the fluorescent yield of element **a** for the shell s = K, L, . . . ;

$F_{a,s}$ is the fraction of photoelectric interactions occurring in the shell s;

$p_l$ is the probability that the fluorescence event belongs to the $l = \alpha, \beta, \gamma, \ldots$ line of interest;

$w_a$ is the weight fraction of element **a**;

$\mu(E_0)$ and $\mu(E_a)$ are the total mass attenuation coefficients of the sample for incident and XRF energy, respectively;

$\rho$ is the physical density and $x$ the thickness of the sample.

In equation (1) contributions resulting from finite incident of the impinging and exit angles are neglected; here it is worth noting that in non-destructive analysis of an object it is difficult to estimate these angles due to the roughness of the surface, which is unknown.

Figure 2 shows the interaction of a monochromatic X-ray beam in a layer ($x$ of a homogeneous sample), giving rise to the production of the secondary fluorescence beam.

In the case of bulk metal artefacts a number of approximations hold:

- the exponential term can be neglected (thick sample approximation);
- the alloy is composed of few major elements (for example copper, tin and lead in the case of a

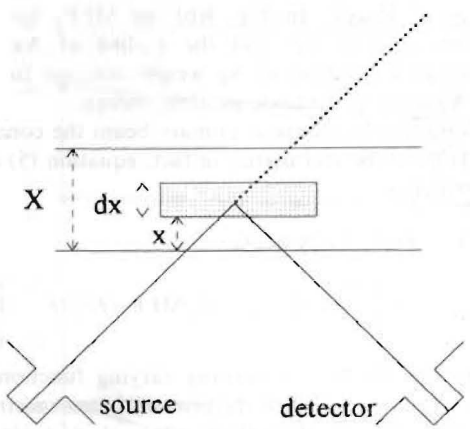


Fig. 2. Interaction of X-ray beam in a layer $dx$ of a homogeneous sample and detection of the secondary fluorescence flux.

bronze) which are at the same time the matrix and the elements to be determined.

In this case a more simple equation can be written

$$N_a = N_0 k \epsilon(E_a) \omega_{a,s} F_{a,s} p_l w_a \frac{\mu_{ph,a}(E_0)}{\mu(E_0) + \mu(E_a)}. \quad (2)$$

The total mass attenuation coefficients can be written as:

$$\mu(E) = \Sigma_i w_i \mu_i(E) \quad (3)$$

where $\mu_i$ is the mass absorption coefficients of element $i$, this being present in the sample with a weight fraction $w_i$. One can then rewrite equation (2) as

$$N_a = N_0 k \epsilon(E_a) \omega_{a,s} F_{a,s} p_l w_a \times \frac{\mu_{ph,a}(E_0)}{\sum_i w_i \mu_i(E_0) + \sum_i w_i \mu_i(E_a)} \quad (4)$$

where, obviously $\sum_i w_i = 1$.

For a polychromatic excitation beam, such as emitted by an X-ray tube, the relationship between $N_a$ and $w_a$ is more complex

$$N_a = k \epsilon(E_a) F_{a,s} p_l \omega_{a,s} w_a \times \int_{E_s}^{E_{Max}} \frac{N_0(E) \mu_{ph,a}(E)}{\sum_i w_i \mu_i(E) + \sum_i w_i \mu_i(E_a)} dE \quad (5)$$

where $E_s$ is the binding energy of the electron in the shell s in which the vacancy occurs and $E_{Max}$ is the upper limit of the exciting spectrum; in the case of an X-ray tube this energy corresponds to the voltage (kV) applied to the X-ray tube.

*The analysed thickness and the mean free path of photons in a EDXRF measure*

One problem in non-destructive analysis of a metal artefact is the determination of the thickness of the sample being probed in the measurement. Using the concept of Mean Free Path (MFP) of a photon in a homogeneous material it is possible to give a value to the probed thickness. The concept of MFP can be useful in describing the absorption of X-rays across a target, and can also be used in describing the emission of fluorescent radiation.

The MFP is defined as the mean path of a photon before an interaction

$$MFP(E) = \frac{\int_0^\infty x e^{-\mu_l(E)x} dx}{\int_0^\infty e^{-\mu_l(E)x} dx} = \frac{1}{\mu} \quad (6)$$

where $\mu_l(E)$ is the linear absorption coefficient of the target at the energy $E$ of the incoming photon. For a thickness equal to one MFP the intensity of the primary beam decreases by the factor 1/e, i.e. by 63.2%.

Substituting for mass with the linear absorption coefficients in equation (1) we obtain:

$$N_a = N_0 k \epsilon(E_a) \mu_{ph,a}(E_0) \omega_{a,s} F_{a,s} p_l w_a \rho \times \frac{1 - e^{-(\mu_l(E_0) + \mu_l(E_a))\rho x}}{\mu_l(E_0) + \mu_l(E_a)} \quad (7)$$

where $\mu_l(E_0)$ and $\mu_l(E_a)$ are the linear attenuation coefficients of the sample at incident and fluorescent X-ray energy, respectively, and $\rho$ is the density of the material.

Using the definition of MFP

$$\mu_l(E_0) + \mu_l(E_a) = \frac{1}{MFP(E_0)} + \frac{1}{MFP(E_a)} \quad (8)$$

and introducing the concept of total $MFP_T$ in the process

$$\frac{1}{MFP_T} = \frac{1}{MFP(E_0)} + \frac{1}{MFP(E_a)} \Rightarrow MFP_T = \frac{MFP(E_0) \cdot MFP(E_a)}{MFP(E_0) + MFP(E_a)} \quad (9)$$

it is possible rewrite equation (7) as follows:

$$N_a = N_0 k \epsilon(E_a) \mu_{ph,a}(E_0) \omega_{a,s} F_{a,s} p_l w_a \times \rho MFP_T \left(1 - e^{\frac{x}{MFP_T}}\right). \quad (10)$$

Therefore, the intensity of fluorescent radiation is a function of the MFP. In particular, a thickness equal to one $MFP_T$ yields 63.2% of the total intensity; therefore, $MFP_T$ is a good measure of the probed thickness of the material.

In a target having a thickness greater then 4.6 $MFP_T$ the exponential term can be neglected and

equation (10) becomes:

$$N_a = N_0 k\epsilon(E_a)\mu_{ph,a}(E_0)\omega_{a,s}F_{a,s}\,p_l w_a \rho \mathrm{MFP}_T. \quad (11)$$

Since necessarily $E_0 > E_a$, it can be easily demonstrated that:

$$\mathrm{MFP}(E_a) < \mathrm{MFP}_T < \mathrm{MFP}(E_0)/2 \quad (12)$$

$\mathrm{MFP}_T$ being equal to $\mathrm{MFP}(E_0)/2$ for the coherent scattering only, when the energy of the incoming photon is equal to that of the exiting.

There are only a few exceptions to the statement that $\mathrm{MFP}(E_a) < \mathrm{MFP}(E_0)$. This happens restrictively when the exciting energy is just below an absorption edge of a major element of the alloy. In this case the probed volume is determined by the small penetration of exciting beam.

Figure 3 shows the MFP values (for the energies of the $K_\alpha$-lines of the elements in the interval $20 \le Z \le 60$) for four typical elements with which the ancient metal artefacts were manufactured. The MFPs are always less than 200 $\mu$m, this also being the case for the $K_\alpha$-lines of higher-$Z$ elements, such as Sn and Sb. For an Au matrix the MFPs are very low, especially for elements such as Fe and Cu; in this case only a very superficial layer is probed; therefore any treatment or degradation of the surface can produce significant effects.

The MFP depends upon the weight fraction of the constituents of the alloy; in Fig. 4(a) the $\mathrm{MFP}_T$ for the $K_\alpha$-lines of Cu, Ag, Sn are shown, as is that for the $L_\alpha$-line of Pb, as a function of Sn weight fraction for a Cu-Sn alloy and for an exciting energy of 31 keV. In Fig. 4(b) the $\mathrm{MFP}_T$ for the $K_\alpha$-lines of Cu, Ag, and the $L_\alpha$-line of Au are shown as a function of Ag weight fraction for an Au–Ag alloy at the same incident energy.

Using a polychromatic primary beam the concept of MFP can be still useful; in fact, equation (5) can be written as:

$$N_a = k\epsilon(E_a)F_{a,s}p_l\omega_{a,s}w_a \times \int_{E_a}^{E_{Max}} N_0(E)\mu_{ph,a}(E)\mathrm{MFP}_T(E)\,dE \quad (13)$$

where the $\mathrm{MFP}_T$ is a slowing varying function of the energy (except when the primary beam spectrum encompasses an absorption edge of a majority element of the alloy) and both $\mu_{ph,a}$ and $N_0(E)$ are rapidly varying functions of the energy. It is therefore possible to introduce an effective $\mathrm{MFP}_T$

$$\mathrm{MFP}_T = \int_{E_a}^{E_{Max}} N_0(E)\mathrm{MFP}_T(E)\,dE. \quad (14)$$

The interval of variability of the $\mathrm{MFP}_T$ can be calculated using equation (12)

$$\mathrm{MFP}(E_a) < \mathrm{MFP}_T < \mathrm{MFP}(E_{Max})/2. \quad (15)$$

*The fundamental parameter and the ratio of the peaks methods*

The fundamental parameters method is a well known approach for quantitative analysis in X-ray emission spectrometry, both using charged particles (electrons, Gedcke *et al.*, 1982 and

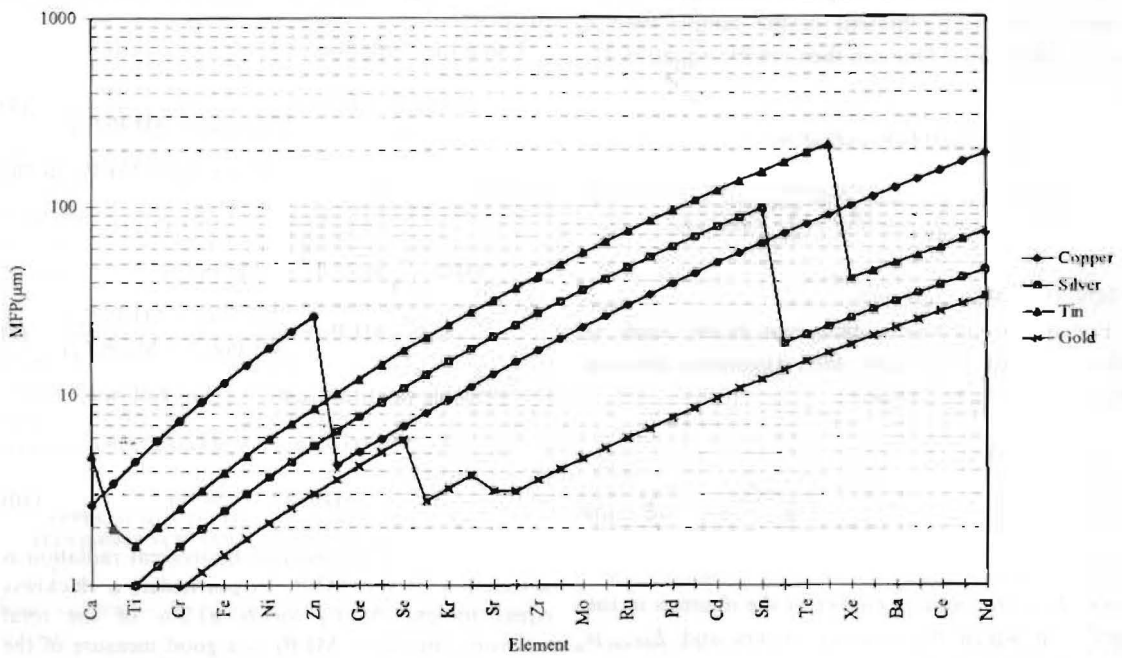


Fig. 3. Total Mean Free Paths (see equation (9)) for the energies of the $K_\alpha$-lines of the elements in the interval $20 \le Z \le 60$ for four typical elements with which the ancient metal artefacts were manufactured.

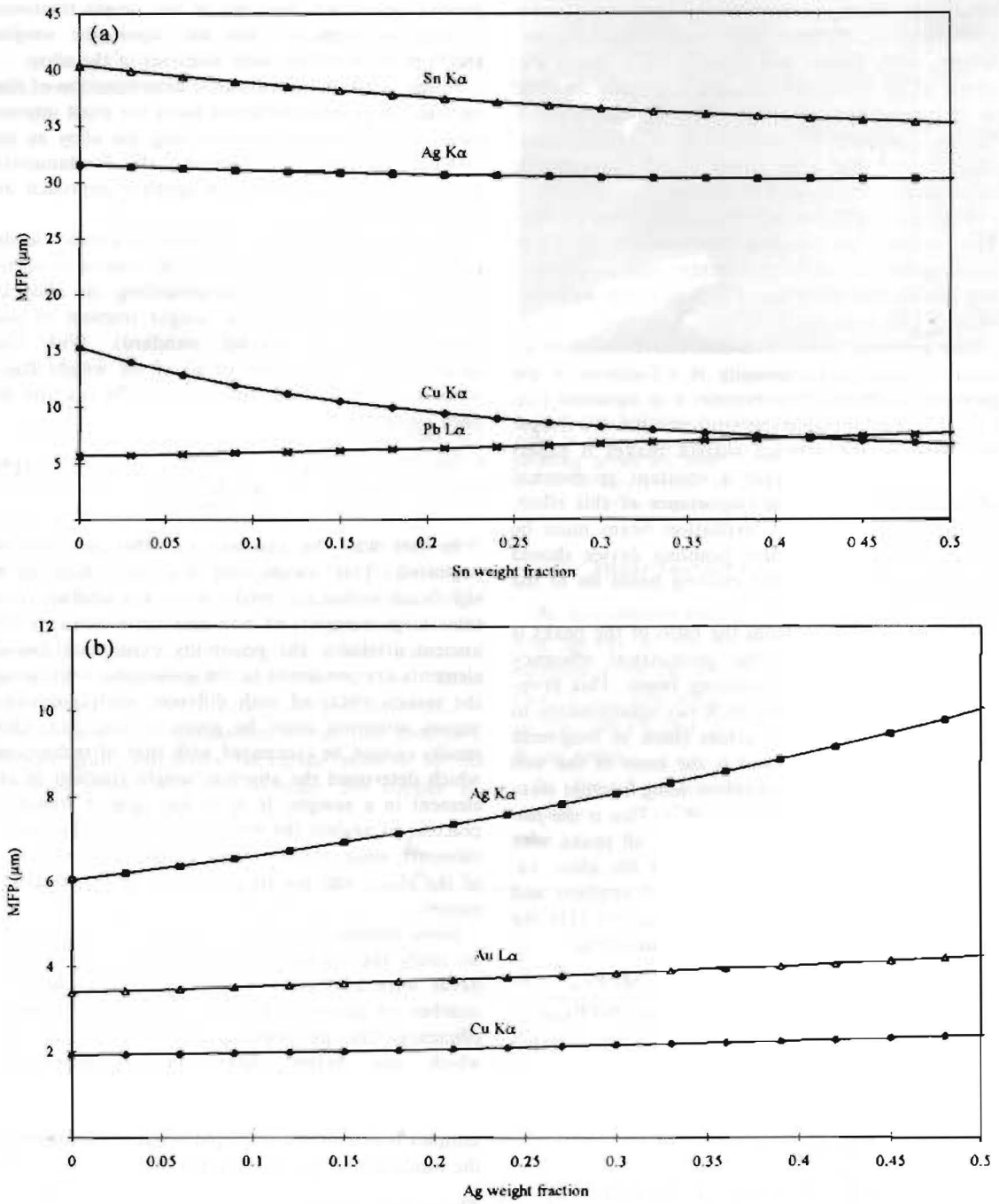


Fig. 4. (a) $MFP_T$ (exciting energy 31 keV) for the $K_\alpha$-lines of Cu, Ag, Sn and the $L_\alpha$-line of Pb as a function of Sn weight fraction for a Cu-Sn alloy; (b) $MFP_T$ (exciting energy 31 keV) for the $K_\alpha$-lines of Cu, Ag, and the $L_\alpha$-line of Au as a function of Ag weight fraction for an Au–Ag alloy.

protons, Maxwell *et al.*, 1988) and photons (Van Espen *et al.*, 1977; Shen and Russ, 1977). For non-destructive EDXRF analysis of ancient metal alloys, the usefulness of the technique is very clear. In fact, since concentrations of elements constituting the alloys can be extremely variable, the response curves are non-linear and this restricts the possibility of obtaining a precise interpolation. In addition, it is difficult to have a good set of standard samples for each application.

This method uses the fundamental equations given in the section 'Basic equations for quantitative X-ray fluorescence analysis' to calculate the weight fraction of each element. To do this the

tabulated values of the partial and total mass absorption coefficients are used (Hubbell and Seltzer, 1995; Berger and Hubell, 1987; Storm and Israel, 1970) as are the physical constants involved in the production of a fluorescence event, such as fluorescence yield (Bambynek *et al.*, 1974), transition probability, edge jumps of the photoelectric cross sections (Scofield, 1973), etc.

With this approach only a small number of standards samples are required, these being necessary to calculate the values of parameters such as physical and geometrical efficiency, which can only be determined experimentally.

One problem in the non-destructive study of an object is that peaks intensity is a function of the geometrical efficiency (parameter $k$ in equation (1)). Use of a transportable spectrometer and the irregular shape of the artefact surface makes it experimentally difficult to have a constant geometrical efficiency. To reduce the importance of this effect, the size of the primary excitation beam must be minimised and an efficient pointing device should also be used to direct the exciting beam on to the desired point.

In an emission spectrum the ratio of the peaks is always independent of the geometrical efficiency and the intensity of the exciting beam. This property has been widely used in X-ray spectrometry to correct for a number of errors (such as long-term fluctuations and drifts) and is the basis of the well known method of normalisation using internal standards (Klockenkämper *et al.*, 1987). This is the justification for the use of the ratio of all peaks with respect to the most intense peak of the alloy, i.e. copper for the bronzes, gold for gold artefacts and silver for silver artefacts. Using equation (11) the intensity ratio of two peaks can be written as:

$$\frac{N_a}{N_{ref}} = \frac{\epsilon(E_a)\mu_{ph,a}(E_0)\omega_{a,s}F_{a,s}p_l w_a \mathrm{MFP}_{T,a}}{\epsilon(E_{ref})\mu_{ph,ref}(E_0)\omega_{ref,s}F_{ref,s}p_l w_{ref}\mathrm{MFP}_{T,ref}} \tag{16a}$$

or in the case of a polychromatic exciting beam (equation (13))

$$\frac{N_a}{N_{ref}} = \frac{\epsilon(E_a)F_{a,s}p_l\omega_{a,s}w_a \times \int_{E_{s,a}}^{E_{Max}} N_0(E)\mu_{ph,a}(E)MFP_T(E)\,dE}{\epsilon(E_{ref})F_{ref,s}p_l\omega_{ref,s}w_{ref} \times \int_{E_{s,ref}}^{E_{Max}} N_0(E)\mu_{ph,ref}(E)\mathrm{MFP}_T(E)\,dE} \tag{16b}$$

It is necessary to stress that the $\mathrm{MFP}_T$ depends on the sample composition, and therefore each MFP depends on the weight fraction of all the elements constituting the alloy. Looking at Fig. 4(a) it is evident that the ratio of the $\mathrm{MFP}_T$s for Sn and Cu is not constant for an increasing weight fraction of Sn, therefore the ratio of equation (13) does not depend only upon the ratio of the weight fractions of the two elements, but also upon the weight fractions of all of the other elements of the alloy.

In this work the quantitative determination of the ancient alloys was performed using the most intense peak of the element characterising the alloy as an internal standard and applying the fundamental parameter method (using an iterative approach as described below).

Using an element as internal standard leads to the consequence that only the relative concentration of each element compounding the alloy is determined (relative to the weight fraction of the element used as internal standard). With the assumption that the sum of all of the weight fractions must be one, we can calculate the fraction of each element

$$w_a = \frac{w_a/w_{ref}}{1 + \sum_i \frac{w_i}{w_{ref}}} \tag{17}$$

In this way the presence of other elements is neglected. This assumption will only lead to a significant systematic errors when the artefact contains large amounts of non-detectable elements. In ancient artefacts, the possibility exists that low-$Z$ elements are contained in the inclusions; comparing the results obtained with different analytical techniques attention must be given to this fact. Our results cannot be compared with that of techniques which determine the absolute weight fraction of an element in a sample. It is, in any case, a common practice to neglect the weight fraction of the low-$Z$ elements, since, usually, these elements are not part of the alloy, and are frequently a sign of contamination.

Some standard samples have been used in order to verify the reliability of the results. These standards were also used to calculate the value of a number of parameters, such as intrinsic detector efficiency (the parameter $\epsilon(E_a)$ in equation (1)), which are better determined experimentally. However, the possibility of determining the weight fraction of elements for which there are no standard samples is one of the principal attractive features of the fundamental parameters method.

*The iterative approach*

As mentioned before for an alloy composed of $n$ elements it is possible to write a system of equations in which the relative weight fractions ($w_a/w_{ref}$) are unknowns. In the literature one can find several approaches to linearising of the equations and solving for the system. A different approach is to write the equations for all the elements constituting the alloy

$$\frac{w_a}{w_{ref}} = \frac{\epsilon(E_{ref})\mu_{ph,ref}(E_0)\omega_{ref,s}E_{ref,s}F_{ref,s}p_l\mathrm{MFP}_{T,ref}}{\epsilon(E_a)\mu_{ph,a}(E_0)\omega_{a,s}p_l\mathrm{MFP}_{T,a}}\frac{N_a}{N_{ref}} \tag{15b}$$

and calculating the relative weight fraction with an iterative approach. Initially, substitution is made of $(w_i/w_{ref})$ in the values into the right side of the equations, the values being calculated assuming that all the $MFP_T$ are equal. In performing a few iterations the condition

$$(w_1/w_{ref})^n - (w_1/w_{ref})^{n-1} < k_1$$

$$(w_2/w_{ref})^n - (w_2/w_{ref})^{n-1} < k_2$$

$$\ldots\ldots\ldots\ldots\ldots\ldots\ldots\ldots$$

$$(w_n/w_{ref})^n - (w_n/w_{ref})^{n-1} < k_n$$

is fulfilled and in this way the $w_i/w_{ref}$ values are determined. The values for the $k_i$ are fixed in such a way that in practice the residual uncertainty is only a statistical one.

The algorithm developing this approach was implemented using Visual Basic for Applications interconnected with an Excel 5 spreadsheet. The input of the program is the spectrum of the analysed object. Such spectra have been translated from a multichannel exit file to an Excel Spreadsheet through a procedure also developed in Visual Basic for Application. From this spectrum, the program calculates the areas relative to the different peaks. For the bronzes, the copper $K_\alpha$ peak can be used as a reference.

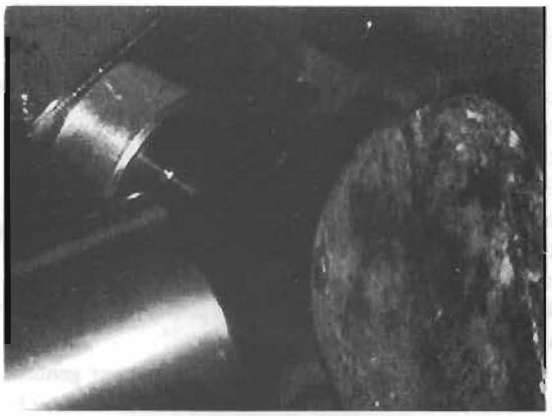

Fig. 5. Photograph of transportable equipment which was used in making measurements on an ancient metal artefact held in the Bologna Archaeological Museum. The X-ray tube, a non-cryogenic detector (Si-PIN) device and the pointing device are both visible. The exciting beam is directed on a very small area through a cylindrical collimator having an exit hole of 2 mm radius.

## EDXRF TRANSPORTABLE EQUIPMENT

As discussed in the Introduction, the two controlling factors in the development of transportable equipment are the availability (a) of room temperature X-ray detectors having an energy resolution of 200–300 eV and (b) of miniaturised low power X-ray tubes.

In Fig. 5 a typical portable spectrometer is shown.

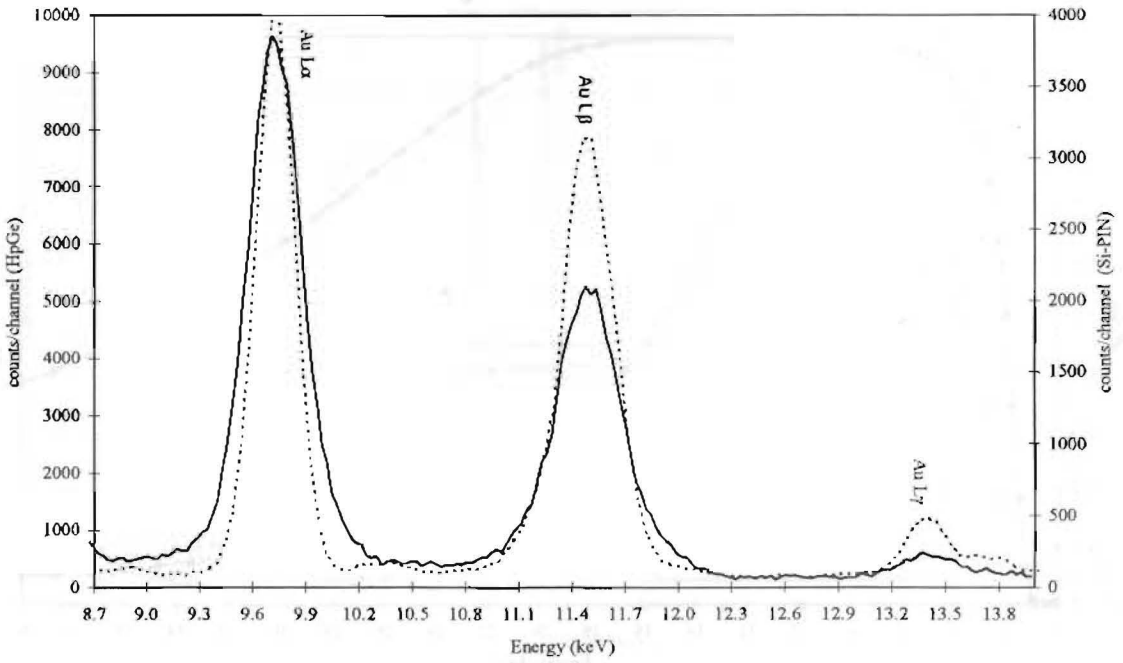


Fig. 6. Spectra of a gold artefact acquired using (a) a HpGe detector and (b) an electrothermally cooled Si-PIN detector. Visual comparison of the two spectra indicates reduced resolution for the non-cryogenic detector.

### X-RAY TUBE

Nowadays, small X-ray tubes are available that can be used in conjunction with portable spectrometers. The principal characteristics of these tubes are: (a) air cooling; (b) low weight; (c) stability. The miniaturisation of a suitable X-ray tube and related power generator is feasible because of the limited requirements for analysis of archaeological samples. In fact, a high voltage supply of 40–45 kV and a current of 200–300 $\mu$A is adequate for such purpose.

A compact X-ray tube with a high power generator has been developed by EIS srl, Rome. The technical characteristics of this source are:

- Tungsten anode
- Focus 0.6 mm (I.E.C.)
- Inherent filtration of 0.8 mm Al
- Stabilised anode HV adjustable in the interval 20–50 kV
- Anode current adjustable in the interval 0–1 mA
- Air cooling
- Dimensions 163 mm (W) × 193 mm (D) × 180 mm (H)
- Weight ~7 kg
- Laser Pointer

The air cooling system is based on the very efficient heat transfer available inside the tube shielding box through convective movements of a non-conductive liquid. In addition, the actual power supply is characterised by very high stability.

*X-ray detectors*

Two types of Peltier-cooled miniaturised detectors were employed, $HgI_2$ and Si-PIN.

The mercuric iodide detector, developed by Iwanczyk and co-workers (Iwanczyk *et al.*, 1984, 1989), is characterised by about 200 eV resolution at 5.9 keV and by very small size and weight, in comparison with cryogenic detectors. This has been employed for in situ analysis of ancient gold and bronze samples; the spectra obtained are quite similar to those of nitrogen cooled Si(Li) or HpGe (see Fig. 6).

Si-PIN detectors have been developed over the last few years, especially by AMPTEK, and are characterised by a 300 $\mu$m Si-diode and cooling with a Peltier cell (Huber *et al.*, 1995). This detector is characterised by an energy resolution of about 250 eV at 5.9 keV. The efficiency of this detector rapidly decreases beyond 25–30 keV, due to the reduced thickness of the Si-diode (see Fig. 7).

### RESULTS

The objective of the currently reported research was to evaluate the feasibility of carrying out measurements in museums on groups of metal artefacts using transportable equipment. In the following, some results obtained during these campaigns will be discussed, followed in the next section by some optimisation criteria for the measuring system.

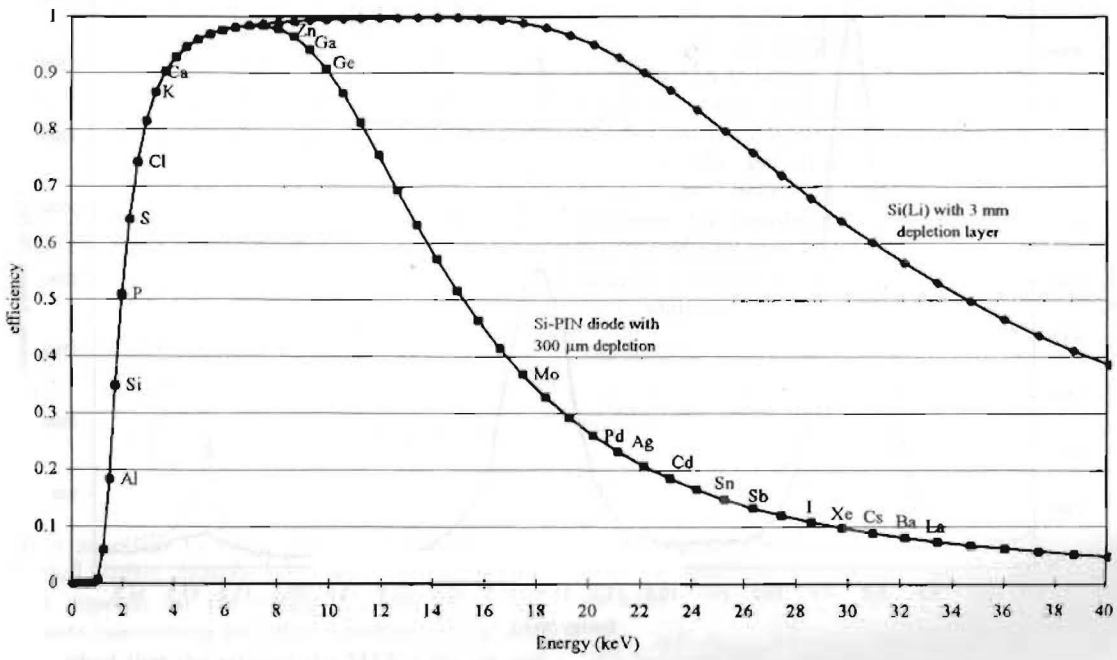


Fig. 7. Efficiency curves for a Si(Li) detector cooled with liquid nitrogen (3 mm thick) and an electrothermally cooled Si-PIN detector (300 $\mu$m thick).

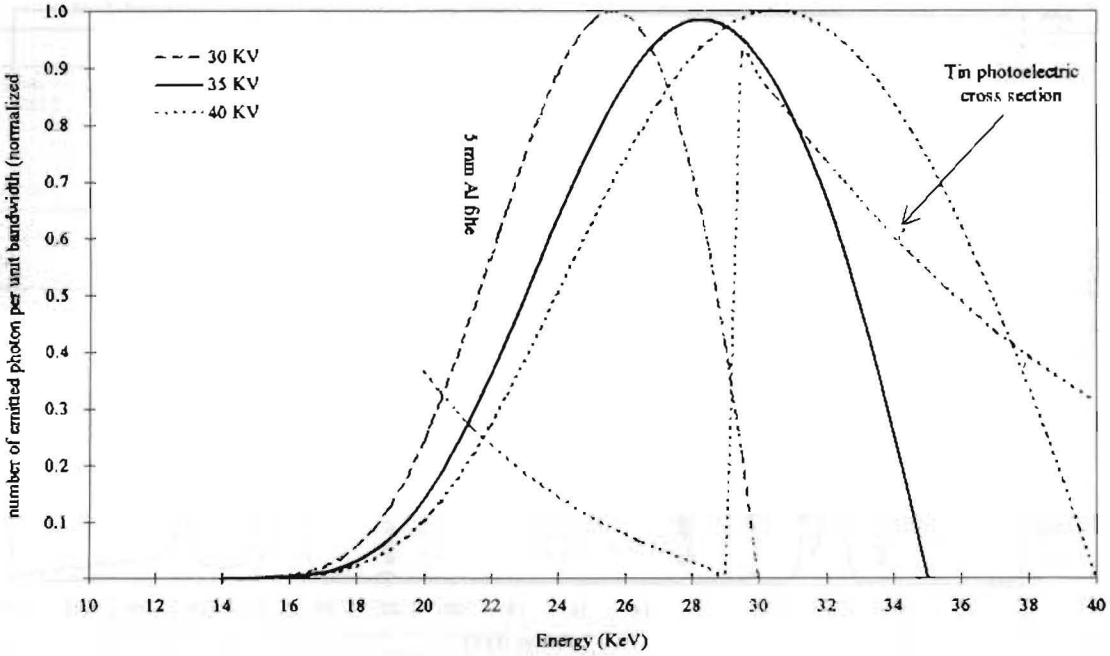


Fig. 8. Simulation of the emission spectra of an X-ray tube with HV of 30-, 35- and 40-kV and 5 mm Al filter.

*Optimisation of measuring conditions*

Optimisation of the exciting energy and source intensity is required to always have an optimal counting rate in the peaks of interest. For this it is necessary to vary the exciting beam spectrum. The high intensity of an X-ray tube allows one to obtain a relatively fine pencil beam (5 to 6 $mm^2$) of variable mean energy in order to excite the fluorescence over a small area of the artefact.

In Fig. 8 simulated spectra for HV of 30-, 35- and 40-kV with a 5 mm Al filter are shown. The simulation shows how the voltage critically influ-

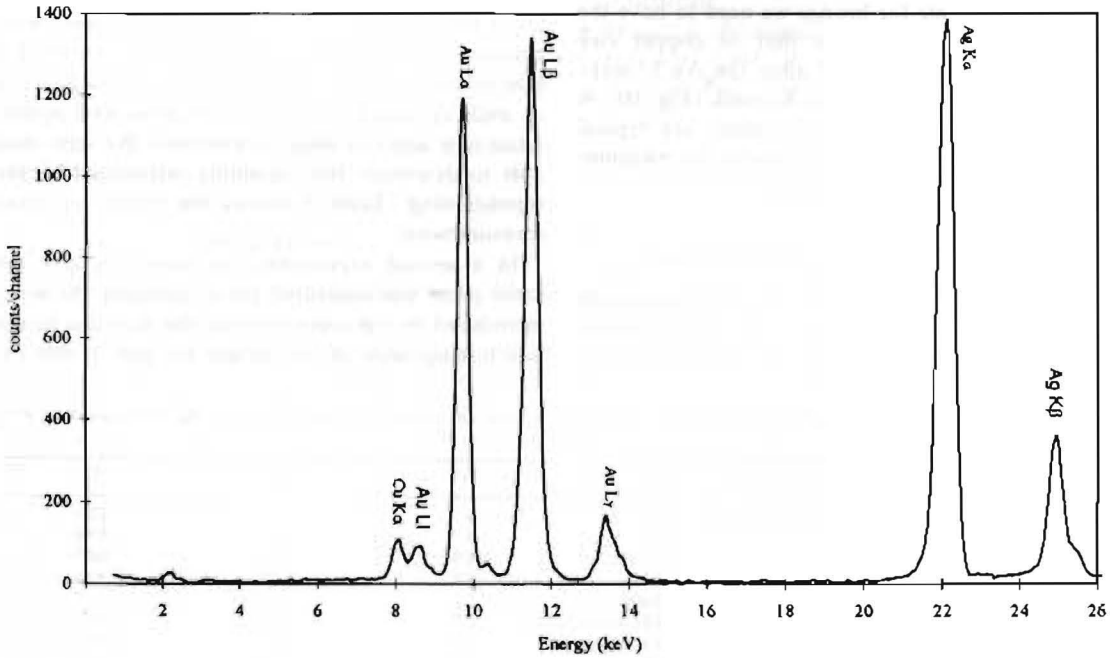


Fig. 9. EDXRF spectrum of an Etruscan item of gold–silver alloy, acquired by the Villa Giulia Museum in Rome. A $HgI_2$ non-cryogenic detector and a miniaturised X-ray tube (HV 35 kV, 500 $\mu$A) were used.

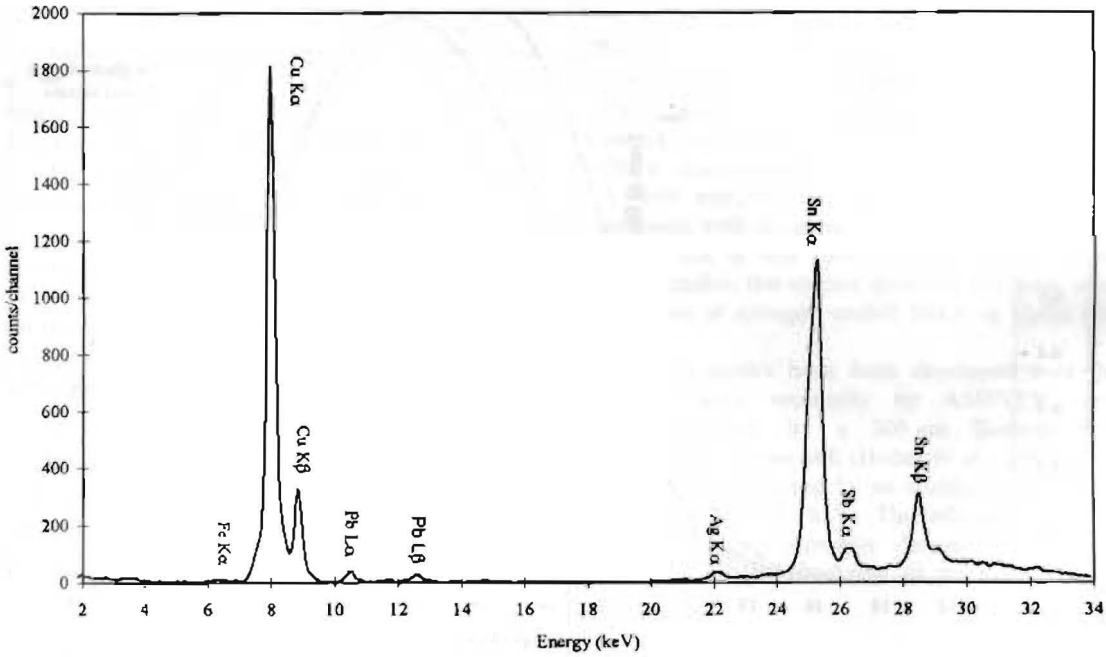


Fig. 10. EDXRF spectrum of a Villanoviano period bronze acquired by the Bolsena Museum. A Si-PIN detector and a miniaturised X-ray tube (HV 40 kV, 500 $\mu$A) were used.

ences the excitation of the elements, including tin, antimony and silver. For the above conditions the absorption edges of these elements are in the middle part of the X-ray tube spectrum. The intensity of the low atomic number elements is not strongly influenced by the X-ray tube voltage.

The optimisation criterion is to have approximately the same peak intensity for the two major elements; for example for bronze we need to have the peak of tin about equal to that of copper (see Fig. 9) and for a gold–silver alloy the Au L-peaks must be about equal to the Ag $K_\alpha$-peak (Fig. 10). A 40 kV HV and a 200–400 $\mu$A current are typical values in order to obtain good results for measurements on bronzes and silver alloys.

*Empirical determination of experimental errors*

The evaluation of errors in non-destructive measurements is made difficult by many contributions which are not easy to estimate. In a measurement of a homogeneous sample with a fixed geometry, the statistical error can be regarded to be the largest source of error.

In addition, two other errors should be evaluated: (a) the positioning of the sample (including surface roughness); (b) non-homogeneity of the sample (i.e. the presence of granular and dendritic microstructures).

To estimate these errors three experiments were performed. In the first, a sample (in the form of a homogeneous ingot) containing 85% of Cu and 5% of each of Zn, Pb and Sn, was measured several times in a series of daily experiments. We were thus able to determine the variability introduced by the repositioning. Table 1 shows the results of these measurements.

In a second experiment, on three artefacts the same point was measured twice, assessing the error introduced by the repositioning plus that due to the non-homogeneity of the sample (in fact in this ex-

Table 1. Results obtained by different measurements on a standard sample containing 5% each of Pb, Zn, Sn. The remaining 85% was Cu

| | Zn | Pb | Sn | Fe | Cu |
|---|---|---|---|---|---|
| stand1-1 | 3.9 | 5.5 | 4.5 | 0.2 | 85.9 |
| stand1-2 | 6.2 | 5.7 | 4.5 | 0.3 | 83.4 |
| stand1-3 | 4.5 | 5.2 | 4.9 | 0.4 | 84.9 |
| stand1-4 | 5.0 | 4.5 | 5.9 | 0.2 | 84.4 |
| stand1-5 | 4.2 | 5.4 | 5.1 | 0.1 | 85.1 |
| stand1-6 | 4.7 | 5.1 | 4.7 | 0.4 | 85.1 |
| stand1-7 | 5.9 | 5.1 | 5.0 | 0.2 | 83.7 |
| stand1-8 | 5.8 | 5.4 | 4.9 | 0.1 | 83.8 |
| stand1-9 | 4.9 | 5.3 | 5.4 | 0.2 | 84.1 |
| average | 5.0 | 5.2 | 5.0 | 0.24 | 84.5 |
| standard deviation | 0.9 | 0.3 | 0.3 | 0.12 | 0.9 |

Table 2. Results obtained in examination of three ancient metal artefacts, from two repeat measurements at the same point

| | Zn | As | Pb | Sn | Fe | Ag | Sb | Cu |
|---|---|---|---|---|---|---|---|---|
| 63344a.1 | 3.5 | 0.3 | 0.8 | 11.1 | 0.4 | 0.1 | 0.2 | 83.6 |
| 63344a.2 | 3.4 | 0.4 | 0.5 | 11.6 | 0.1 | 0.1 | 0.3 | 83.6 |
| 61344a.1 | 4.1 | 0.5 | 0.6 | 7.5 | 0.2 | – | – | 87.1 |
| 61344a.2 | 4 | 0.5 | 0.5 | 6.8 | 0.3 | – | – | 87.9 |
| 61300a.1 | 3.2 | – | 1.4 | 15.1 | 0.2 | – | 0.2 | 79.9 |
| 61300a.2 | 3.1 | 0.4 | 1.1 | 14.7 | 0.4 | – | – | 80.3 |

Table 3. Results obtained examining four ancient metal artefacts, from repeat measurements at different points

| | Zn | As | Pb | Sn | Fe | Ag | Sb | Cu |
|---|---|---|---|---|---|---|---|---|
| 63331a | 3.9 | 0.2 | 2.2 | 17.1 | 0.2 | 0.1 | 0.1 | 76.1 |
| 63331b | 3.6 | 0.1 | 2.0 | 15.7 | 0.5 | 0.1 | 0.1 | 77.9 |
| 63346a | 4.7 | – | 1.1 | 6.9 | 3.5 | – | 0.2 | 83.7 |
| 63346b | 3.7 | 0.2 | 0.3 | 10.5 | 1.2 | – | 0.2 | 83.8 |
| 63346c | 3.4 | 0.1 | 0.6 | 11.1 | 0.8 | 0.1 | 0.3 | 83.7 |
| 61285a | 6.1 | – | 1.0 | 12.1 | 0.4 | – | – | 80.5 |
| 61285b | 5.1 | – | 1.3 | 14.2 | 0.0 | – | – | 79.4 |
| 61283a | 3.7 | – | – | 11.6 | 0.5 | – | 0.3 | 83.9 |
| 61283b | 3.7 | – | 0.3 | 10.3 | 0.2 | 0.3 | 0.5 | 84.7 |
| 61006a | 3.7 | – | 2.7 | 10.8 | 0.4 | – | 0.2 | 82.1 |
| 61006b | 4.2 | 0.6 | 2.3 | 9.2 | 0.5 | – | – | 83.3 |

Table 4. Experimental results obtained by analysing three standard samples, compared with theoretical predictions

| | Zn | | Pb | | Sn | | Cu | |
|---|---|---|---|---|---|---|---|---|
| | theor. | exper. | theor. | exper. | theor. | exper. | theor. | exper. |
| stand.1 | 5.0 | 4.9 | 5.0 | 4.7 | 5.0 | 5.1 | 85.0 | 85.3 |
| stand.2 | – | – | 14.0 | 14.5 | 8.0 | 8.2 | 78.0 | 77.4 |
| stand.3 | - | – | 8.0 | 7.8 | 6.0 | 5.6 | 86.0 | 86.6 |

periment we used an artefact which had an evident granular microstructure). Table 2 shows the results of this experiment.

In a third experiment we carried out measurements on different points of four artefacts: the results of these measurements are shown in Table 3.

Finally, using a set of standard samples it was possible to evaluate the accuracy obtainable with the used method; Table 4 shows the results obtained using the fundamental parameters method. Here the errors introduced appeared less significant than those discussed above.

## APPLICATIONS

The transportable equipment described above was used in measurements carried out by a large interdisciplinary group of scientists (mainly physicists and chemists, but also including archaeologists and archaeometrists). In these studies an approach was developed in which many different techniques were used to examine ancient metals. In particular, the use of EDXRF was combined with the use of the metallography (Giardino *et al.*, 1996), a technique which allows study of the microstructure of the alloys. EDXRF has been applied, over the last 3 years, in the analysis of ancient metals from the following museums:

- Museo Civico of Bolsena on bronzes found at the archaeological site of Gran Carro, near Bolsena lake (Caneva *et al.*, 1996);
- Museo Sanna of Sassari, on metal artefacts and ingots found at three nuragic sites;
- Museo Civico of Bologna, on bronzes from San Francesco (Bietti Sestieri *et al.*, 1998);
- Musei Capitolini in Rome, on silver vessels from Boscoreale;
- Museo Archeologico of Valle Giulia in Rome, on Etruscan gold from the Castellani collection (Caruso *et al.*, 1996).

## CONCLUSIONS

The use of non-cryogenic detectors and miniaturised X-ray tubes are viable in non-destructive EDXRF analysis of ancient metals. As such, transportable EDXRF equipment with favourable characteristics can be assembled.

With such systems it is possible to determine the composition of metal artefacts and to study their production technology, also using other techniques such as metallography (Giardino *et al.*, 1996).

*Acknowledgements*—The authors wish to thank Prof. M. Marabelli, Dr. G. Guida, Dr. C. Giardino, Dr. J. S. Iwanczyck, Dr. A. Dabrowsky and Dr. J. A. Pantazis for their scientific support in this research. The authors were supported in this work by a NATO grant, CRG 900130 and by CNR, Special project for the Conservation of Cultural Heritage

## REFERENCES


Bambynek, W., Crasemann, B., Fink, R. W., Freud, H. U., Mark, H., Swift, C. D., Price, R. E. and Rao, P. V., (1974) X-ray fluorescence yields, Auger and Coster–Kroning transition probabilities. *Review Modern Physics* **44**, 716–813 (1972), erratum in **46**, 853 (1974).

Berger, M. J. and Hubbell, J. H. (1987) XCOM: Photon cross sections on a personal computer. Publ. NBSIR 87-3597, National Bureau of Standards, Gaithersburg, MD.

Bietti Sestieri, A. M., Caneva, C., Giardino, C., Gigante, G. E., Mazzeo, R., Morigi Govi, C., Palmieri, A. and Ridolfi, S. (1997) Production and functions of early Iron Age metal artefacts from the Bologna area: archaeometallurgical research on the bronze hoard from San Francesco (Bologna). *Proceedings of the XIII Congress of UISPP of Forlì*, in press.

Cameron, J. F. and Rhodes, J. R. (1961) X-ray spectrometry with radioactive sources. *Nucleonics* **19**(6), 53.

Caneva, C., Cesareo, R., Giardino, C., Gigante, G. E. and Marabelli, M. (1996) Methodologies de rechercherches pour la paleometallurgie: les metaux du site villanovien du Gran Carro (Bolsena). *Actes du colloque de Archèometrie de Perigueux, Supplement de la Revue d'Archeometrie*, 153.

Caruso, I., Cesareo, R., Giardino, C. and Gigante, G. E. (1996) Nouvelle recherches sur les 'Ors Etrusques' de la collection Castellani. *Actes du colloque de Archèometrie de Perigueux, supplement de la Revue d'Archèometrie*, 157.

Cesareo, R., Frazzoli, F. V., Mancini, C., Marabelli, M. and Sciuti, S. (1972) Rapid ND analysis of ancient bronzes. *International Journal of Applied Radiation and Isotopes* **23**, 198.

Cesareo, R., Gigante, G. E., Iwanczyk, J. S. and Dabrowsky, A. (1992) The use of $HgI_2$ detectors for XRF analysis in archaeometry. *Nuclear Instruments and Methods in Physics Research* **A322**, 583.

Cesareo, R., Gigante, G. E., Canegallo, P., Castellano, A., Iwanczyk, J. S. and Dabrowski, A. (1996a) Applications of non-cryogenic portable EDXRF systems in archaeometry and conservation. *Nuclear Instruments and Methods in Physics Research* **B380**, 440.

Cesareo, R., Gigante, G. E., Castellano, A., Rosales, M. A., Aliphat, M., De La Fuente, F., Meitin, J. J., Mendoza, A., Iwanczyk, J. S. and Pantazis, J. A. (1996b) Portable systems for energy dispersive X-ray fluorescence analysis of works of art. *Journal of Trace and Microprobe Techniques* **14**(4), 711.

Gedcke, D. A., Byers, L. G. and Hardy, W. H. (1982) ZAP—A standardless x-ray microanalysis computer program. *Scanning Electron Microscopy* **3**, 981.

Giardino, G., Gigante, G. E., Guida, G. and Mazzeo, R. (1996) *In situ* simultaneous use of energy-dispersive X-ray fluorescence analysis and metallographic analysis applied on archaeological metal artefacts. *Proceedings of the 5th International Conference on Non-destructive Testing, Microanalytical Methods and Environmental Evaluation for Study and Conservation of Works of Art*, Budapest, 24–28 September, p. 327.

Iwanczyk, J. S., Dabrowski, A. J., Huth, G. C. and Drummond, W. (1984) Continuing development of mercuric iodide x ray spectrometry. *Advances in X-Ray Analysis* **27**, 405.

Iwanczyk, J. S., Warburton, W. K., Dabrowski, A. J., Hedman, B., Hodgson, K. O. and Patt, B. E. (1989) Performances and durability of $HgI_2$ x-ray detectors for space missions. *IEEE Transactions on Nuclear Science* **36**(1), 841.

Hubbell, J. H. and Seltzer, S. M. (1995) Tables of x-ray mass attenuation coefficients and mass energy-absorption coefficients 1 keV to 29 MeV for elements Z = 1 to 92 and 48 additional substances of dosimetric interest. National Institute of Standards and Technologies Report NISTIR 95-5632.

Huber, A. C., Pantazis, J. A. and Jordanov, V. T. (1994) High performance, thermoelectrically cooled X-ray and gamma ray detectors Invited paper at the International Conference on Application of Accelerators in Research and Industry, Denton, TX, USA.

Huber, A. C., Pantazis, J. A. and Jordanov, V. (1995) High performance, thermoelectrically cooled X-ray and gamma ray detectors. *Nuclear Instruments and Methods in Physics Research* **B99**, 665.

Klockenkämper, R., Raith, B., Divoux, S., Gonsior, B., Brüggerhoff, S. and Jackwerth, E. (1987) Comparison of different excitation methods for X-ray spectral analysis. *Fresenius Zeitschrift für Analytische Chemie* **326**, 108.

Maxwell, J. A., Campbell, J. L. and Teesdale, W. J. (1988) The Guelph PIXE software package. *Nuclear Instruments and Methods* **B43**, 218.

Oxford Instruments Inc. (1996) 275 Technology Circle, Scotts Valley, CA 95066, USA.

Shen, R. B. and Russ, J. C. (1977) Processing of energy-dispersive X-ray spectra. *Spectrometry* **6**(1), 56.

Storm, E. and Israel, H. I. (1970) Photon cross-sections from 1 keV to 100 keV for elements Z = 1 to 100. *Nuclear Data Tables* **A7**, 565.

Scofield, J. H. (1973) Theoretical photoionization cross sections from 1 to 1500 keV. Lawrence Livermore National Laboratory publication UCRL-51326.

Van Espen, P., Nullens, H. and Adams, F. (1977) A computer analysis of x-ray fluorescence spectra. *Nuclear Instruments and Methods* **142**, 243.

Wang, Y. J., Iwanczyk, J. S. and Graham, W. R. (1993) Evaluation of $HgI_2$ detectors for lead detection in paint. *IEEE Transactions on Nuclear Science* **40**(4), 846.